



Submitted to

---

**32nd International Conference on High Energy Physics, ICHEP04**, August 16, 2004, Beijing

Abstract: **5-0161**

Parallel Session **5**

---

[www-h1.desy.de/h1/www/publications/conf/conf\\_list.html](http://www-h1.desy.de/h1/www/publications/conf/conf_list.html)

## **Determination of the longitudinal proton structure function $F_L$ at low $Q^2$ at HERA**

### **H1 Collaboration**

#### **Abstract**

An extraction of the longitudinal proton structure function  $F_L(x, Q^2)$  from H1 data at low  $Q^2 \sim 1 \text{ GeV}^2$  is reported. The analysis is based on the data collected in a dedicated low  $Q^2$  running period in 1999 and during shifted vertex runs in 2000. Two methods of extracting  $F_L(x, Q^2)$  are discussed. It is shown that results from both methods are consistent. Theoretical predictions are compared with the measured  $F_L(x, Q^2)$  points.

# 1 Introduction

Precise measurements of the inclusive scattering cross section at the  $ep$  collider HERA are important for the understanding of proton substructure. In the one-photon exchange approximation, which is valid in the kinematic domain explored here, the deep inelastic scattering (DIS) cross section is given by the expression:

$$\frac{d^2\sigma}{dx dQ^2} = \frac{2\pi\alpha^2}{Q^4 x} Y_+ (F_2(x, Q^2) - y^2 F_L(x, Q^2)),$$

where  $Y_+ = 1 + (1 - y)^2$ ,  $Q^2$  is the squared four-momentum transfer,  $x$  denotes the Bjorken scaling variable,  $y = Q^2/sx$  is the inelasticity, with  $s$  the  $ep$  center of mass energy squared and  $\alpha$  is the fine structure constant. The structure functions  $F_2$  and  $F_L$  are related to the cross sections  $\sigma_T$  and  $\sigma_L$  for the interaction of transversely and longitudinally polarized photons with protons:

$$F_2(x, Q^2) = \frac{Q^2}{4\pi^2\alpha} (\sigma_T(x, Q^2) + \sigma_L(x, Q^2)), \quad (1)$$

$$F_L(x, Q^2) = \frac{Q^2}{4\pi^2\alpha} (\sigma_L(x, Q^2)). \quad (2)$$

Due to the positivity of the cross sections, the structure functions  $F_2$  and  $F_L$  obey the relation:

$$0 \leq F_L \leq F_2. \quad (3)$$

The “reduced” cross section is defined as:

$$\sigma_r = F_2(x, Q^2) - \frac{y^2}{Y_+} \cdot F_L(x, Q^2). \quad (4)$$

In the Quark Parton Model [1] the photon interacts with a spin 1/2 particle having only longitudinal momentum, which leads to the so called Callan-Gross relation [2]:  $F_L(x) = 0$ . In QCD quarks interact through gluons, which can split into quark anti-quark or gluon pairs. This way, the quark struck by a virtual photon has transverse momentum  $\sim Q$ , which leads to  $F_L(x, Q^2) > 0$ . Due to its origin  $F_L$  is directly connected with the gluon distribution in the proton and therefore can provide a sensitive test of perturbative QCD.

In recent years HERA structure function analyses have focussed on the measurement of  $F_2$  which is the dominating contribution to the inclusive cross section. In these measurements an assumption was made on  $F_L$ , and  $F_2$  was obtained in a wide range of  $x$ ,  $Q^2$  and for inelasticities  $y$  from about 0.6 down to 0.002. At high  $y$ , beyond 0.6, the  $F_L$  contribution to the reduced cross section becomes significant. Therefore, the standard procedure of extracting  $F_2(x, Q^2)$  from the DIS cross section by subtracting the theoretically computed  $F_L$  contribution can be reversed: at high  $y$  the  $F_L(x, Q^2)$  contribution may be extracted from the measured cross section by subtracting a calculation of  $F_2$ .

The H1 cross section measurements access  $y$  values as high as 0.9 since the modified backward apparatus, a silicon strip detector and a Spaghetti calorimeter with a drift chamber attached, enable scattered electrons to be identified down to 3 GeV energy. This allowed the longitudinal structure function to be accessed using different methods developed to determine

$F_2$ . In this paper the new H1 low  $Q^2$  data [3], from dedicated runs in 1999 and with a vertex position shifted in 2000, are used to obtain rather accurate new data on  $F_L$  in the low  $Q^2$  region,  $Q^2 \sim 1 \text{ GeV}^2$ , where no data are available at small Bjorken  $x$  but the theoretical uncertainties are particularly large [4].

The  $F_L$  data are obtained using two methods, the derivative method [5, 6] introduced previously and a new “shape method” which employs the characteristic  $y^2$  dependence in the cross section eq. 1 in order to separate the  $F_2$  and  $F_L$  terms.

## 2 Data and extraction methods

The low  $Q^2$  data used in this study were collected with the H1 detector at HERA in a dedicated running period in 1999 and during shifted vertex runs in 2000. Details concerning data selection and cross section analysis can be found elsewhere [3]. The cross section measured in various  $Q^2$  bins is shown in Fig. 1. For fixed  $Q^2$ , the cross section rises with decreasing  $x$ . However, at very low  $x$  (high  $y$ ) a characteristic bending of the cross section can be noticed. This occurs at all  $Q^2$  values at fixed  $y \sim 0.5$  and is attributed to the contribution from the longitudinal structure function  $F_L(x, Q^2)$ .

### 2.1 $F_L$ extraction with a derivative method

For the  $F_L(x, Q^2)$  extraction from the cross section the data are rebinned in  $Q^2$  taking into account systematic error correlations. A method was used, called the derivative method, introduced in [3, 5]. This method is based on the partial derivative of the reduced cross section calculated at fixed  $Q^2$ ,

$$\left( \frac{\partial \sigma_r}{\partial \ln y} \right)_{Q^2} = \left( \frac{\partial F_2}{\partial \ln y} \right)_{Q^2} - F_L \cdot y^2 \cdot \frac{2-y}{Y_+^2} - \frac{\partial F_L}{\partial \ln y} \cdot \frac{y^2}{Y_+}. \quad (5)$$

At large  $y$  the  $F_L$  contribution to the derivative is of similar size as the  $F_2$  contribution. Thus  $F_L$  can be extracted as the difference between the cross section derivative and the contribution of  $\partial F_2 / \partial \ln y$ , which is estimated by a straight line fit at low  $y \leq 0.2$  [5, 6].  $\partial F_L / \partial \ln y$  is found to be smaller than the error of the  $\partial F_2 / \partial \ln y$  term [6], and it is neglected.

In Fig. 2 the derivative of the reduced cross section for the 2000 low  $Q^2$  data is shown. For illustration also the line fit to the low  $y$  points and its extrapolation to the high  $y$  region, representing the subtracted  $F_2$  derivation, is plotted. The  $F_L(x, Q^2)$  data obtained from the 2000 shifted vertex data are shown in Fig. 3.

The uncertainty of the line fit and its extrapolation, taking into account the correlation of errors at low  $y$  with those at high  $y$ , are included into the systematic errors. Also the error due to neglecting the  $F_L$  derivative term is added considering its calculated size as the resulting error.

The derivative method assumes a linear behaviour of  $\partial F_2 / \partial \ln y$  with  $\ln y$  and extrapolates the information about  $F_2(x, Q^2)$  from the low  $y$  to the high  $y$  region. It does not make full use

of the information provided by the cross section measurement in the intermediate  $y$  region, i.e. for the linear fit the lowest  $y$  points are used but the extraction is made only for the points with highest  $y$ , thus at medium  $y$  some cross section points are not used. The result on  $F_L$  consists in a few points close in  $y$  with sizeable errors. The precision of the measurement does not allow to resolve the  $x$  dependence of  $F_L(x, Q^2)$  on this basis, see Fig. 3. Thus, a new, more precise method for the  $F_L(x, Q^2)$  extraction was developed.

## 2.2 $F_L$ extraction with a shape method

The new method employs the shape of the reduced cross section distribution in a given  $Q^2$  bin, which is governed by the  $y^2$  dependence (Eq. 1), and therefore it is called the shape method. The shape of the reduced cross section at high  $y$  (Fig. 1) is driven by the kinematic factor  $y^2/Y_+$ , and to a lesser extent by  $F_L(x, Q^2)$  which is considered to be constant ( $F_L = F_L(Q^2)$ ), for each  $Q^2$  bin in the narrow  $x$  range, high  $y$  range of sensitivity to  $F_L$  governed by the  $y^2$  term. The method furthermore assumes, in agreement with previous measurements [7], that the structure function  $F_2(x, Q^2)$  behaves like  $x^{-\lambda}$  at fixed  $Q^2$ . On this basis the reduced cross section distribution in each  $Q^2$  bin can be parametrised and fitted as:

$$\sigma_{FIT} = c \cdot x^{-\lambda} - \frac{y^2}{1 + (1 - y)^2} F_L. \quad (6)$$

Fig. 4 illustrates that this fit provides an excellent description of the reduced cross section in the full kinematic range. The  $\lambda$  and  $c$  values extracted from this fit turn out to be in good agreement with previous measurements [7].

For different  $Q^2$  bins the  $F_L(x, Q^2)$  points are thus determined from the fit and a bin-centre procedure is applied to obtain the correct  $x$  value. Statistical uncertainties of the  $F_L$  determination include errors of the fit to the cross section points with their statistical and uncorrelated systematic errors. The correlated systematic errors are treated separately and added in quadrature to the total error. The  $F_L(x, Q^2)$  points, as obtained with the shape method, are compared with the values obtained with the derivative method in Figs. 5 and 6. The results from both approaches are consistent. However, the errors from the shape method turn out to be significantly smaller than those from the derivative method. Therefore, as the final result of this analysis, only the  $F_L$  points extracted with the shape method are used.

## 3 Results

The longitudinal structure function  $F_L(x, Q^2)$  as determined from the 1999 minimum bias and the 2000 shifted vertex H1 data is shown in Fig. 7 together with predictions of different theoretical models. The GBW dipole model [8] is a model based on the concept of saturation for small  $Q^2$  and small  $x$ , which includes only three parameters to describe the DIS data. This model gives a good description of the extracted  $F_L$  points over the whole kinematic region covered by this measurement. The BKS (GRV off-shell) model [9] is based on the photon-gluon fusion mechanism extrapolated to the region of low  $Q^2$  and employing the soft pomeron exchange

mechanism for describing quarks of limited transverse momentum. This model gives a correct description of the data as well.

Fig. 8 shows the same H1 data, together with previously published H1 results, compared here with higher-order QCD fits from H1 [5], ZEUS [10], MRST [4] and Alekhin [11]. The values of  $F_L(x, Q^2)$  are consistent with the previous determination of  $F_L$  by the H1 Collaboration, but are more precise and extend the kinematical region, in which  $F_L(x, Q^2)$  is determined, to the lower  $Q^2$  region. As can be seen there is a significant uncertainty for the  $F_L$  prediction in the NLO QCD fits reflecting the uncertainty of the initial gluon distribution. The H1 data clearly favour a positive, not small  $F_L$  at low  $Q^2$  and small  $x$ , as is preferred by the H1 and Alekhin's fits while the MRST and ZEUS predictions are low <sup>1</sup>. A negative  $F_L$  at small  $x$  is experimentally ruled out, both from the extracted  $F_L$  values, fig. 8, and basically by the measured turn-over of the reduced cross section, fig. 4. It becomes evident from fig. 8 that the  $x$  dependence of  $F_L$  needs to be measured which requires to operate HERA at reduced proton beam energy [13]. The low  $Q^2$  region,  $Q^2 < 5 \text{ GeV}^2$ , will be accessible only in a dedicated new phase of HERA as it requires to rearrange the interaction region.

An overview of all current H1 data on  $F_L(x, Q^2)$ , from  $Q^2 = 0.75 \text{ GeV}^2$  to  $Q^2 = 700 \text{ GeV}^2$  and for fixed  $W=276 \text{ GeV}$ , is given in Fig. 9. It comprises the preliminary results of the low  $Q^2$  analysis described in this paper and the results based on data collected in 96/97 [5] and also the recently published high  $Q^2$  results from  $e^+p$  and  $e^-p$  data [12]. The experimental points are in good agreement with the GBW dipole model [8] in the whole  $Q^2$  range. The BKS (GRV off-shell) model [9], which evolves steeper at low and moderate  $Q^2$ , is still able to describe the data. The H1 QCD fit agrees with the data in the  $Q^2$  region of its applicability beyond a few  $\text{GeV}^2$  while its backward extrapolation exceeds the data for  $Q^2 < 1 \text{ GeV}^2$ .

Fig. 10 presents the  $Q^2$  dependence of  $F_L$  in comparison with the higher order QCD fits. All QCD fits describe the data at larger  $Q^2$  while at lower  $Q^2$  similar conclusions can be drawn as for the  $x$  dependence discussed above.

## 4 Summary

Two methods of extraction of the longitudinal structure function  $F_L(x, Q^2)$  from H1 inclusive cross section data in the low  $Q^2$  region are presented. The derivative method assumes that  $\partial F_2 / \partial \ln y$  is linear in  $\ln y$  and extrapolates the behaviour of  $F_2(x, Q^2)$  from the low  $y$  to the high  $y$  region. The newly introduced shape method approximates the  $F_2(x, Q^2)$  behaviour with  $c \cdot x^{-\lambda}$  at fixed  $Q^2$  and assumes that  $F_L(x, Q^2)$  can be treated as constant, for a given  $Q^2$  bin, in the narrow  $x$  range accessible to this measurement. It is shown that both methods give consistent results, however, the shape method proves to be more precise than the derivative one.

The measured data points are in agreement with previous results and allow to extend the region in which  $F_L$  is extracted into the very low  $Q^2$  region. The strong  $y$  dependence observed

---

<sup>1</sup>Note that none of the QCD fits included low  $x$  data for  $Q^2$  around  $1 \text{ GeV}^2$  which is the edge of the DIS region. The initial distributions usually are parametrised at larger  $Q_0^2$ . The minimum  $Q^2$  of data included is (3.5, 2.5, 2.5, 2)  $\text{GeV}^2$  for H1, ZEUS, Alekhin and MRST while the  $Q_0^2$  is (4, 7, 9, 1)  $\text{GeV}^2$ , respectively. Apart from the MRST fit, all QCD fits are thus backward extrapolated for most of the  $F_L$  data points presented here.

for the cross section at high  $y$  leads to positive results of the longitudinal structure function down to lowest  $Q^2 \sim 1 \text{ GeV}^2$ . This requires the gluon distribution to be positive at lowest  $x$ . Collecting all H1 results,  $F_L(x, Q^2)$  data are presented in a wide  $Q^2$  range, from 0.75 to 700  $\text{GeV}^2$ . A measurement of the  $x$  dependence of  $F_L(x, Q^2)$ , independent of assumptions on  $F_2(x, Q^2)$  and more accurately, can be performed at HERA with a variation of the proton beam energy.

## References

- [1] J. D. Bjorken, Phys. Rev. **179** (1969) 1547.
- [2] C. G. Callan and D. J. Gross, Phys. Rev. Lett. **22** (1969) 156.
- [3] H1 Collaboration, contributed paper 799 to EPS 2001, Budapest.  
H1 Collaboration, contributed paper 979 to ICHEP 2002, Amsterdam.
- [4] A. Martin, R. G. Roberts, W. J. Stirling and R. S. Thorne, Eur. Phys. J. C **23** (2002) 73 [hep-ph/0110215].  
A. Martin, R. G. Roberts, W. J. Stirling and R. S. Thorne, Phys. Lett. B **531** (2002) 216 [hep-ph/0201127].
- [5] C. Adloff *et al.* [H1 Collaboration], Eur. Phys. J. **C21** (2001) 33 [hep-ex/0012053].
- [6] D. Eckstein, Doctoral Thesis, Humboldt University of Berlin, 2002 [DESY-THESIS-2002-008].
- [7] C. Adloff *et al.* [H1 Collaboration], Phys. Lett. B **520** (2001) 183 [hep-ex/0108035].
- [8] K. Golec-Biernat and M. Wüsthoff, Phys. Rev. D **59** (1999) 014017 [hep-ph/9807513].
- [9] B. Badelek, J. Kwieciński and A. Staśto, Z. Phys. C **74** (1997) 297 [hep-ph/9603230].
- [10] S. Chekanov *et al.* [ZEUS Collaboration], Phys. Rev. D **67** (2003) 012007 [hep-ex/0208023].
- [11] S. I. Alekhin Phys. Rev. D **68** (2003) 114002 [hep-ph/0211096].
- [12] C. Adloff *et al.* [H1 Collaboration], Accepted by Eur. Phys. J. C, [hep-ex/0304003].
- [13] L. Bauerdick, A. Glazov and M. Klein, Proc. Workshop on Future Physics at HERA, eds. G. Ingelmann, A. De Roeck and R. Klanner, Hamburg DESY 77 (1996) [hep-ex/9609017].

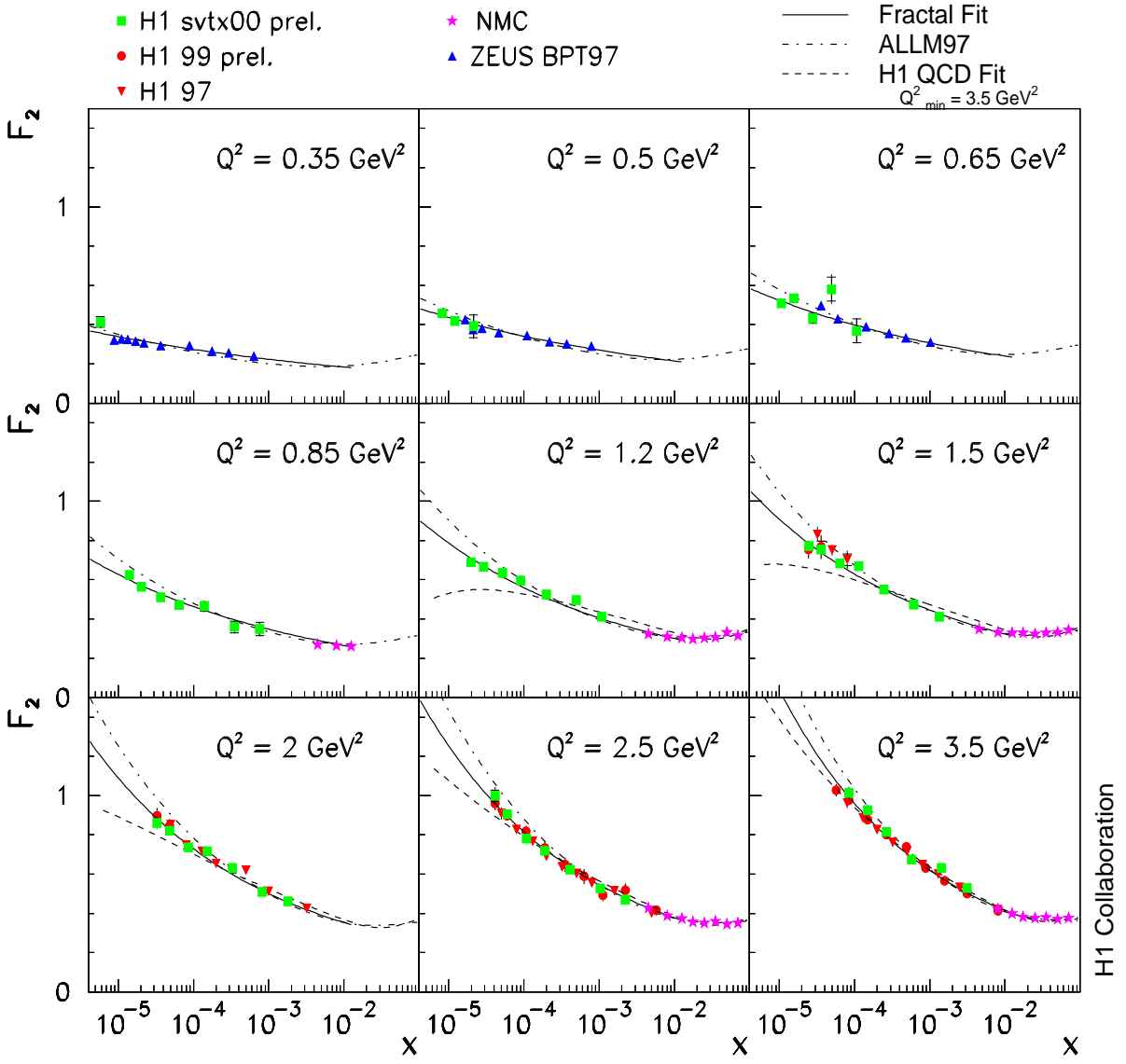


Figure 1: Measurements of the inclusive DIS cross section for the 1999 minimum bias and the 2000 shifted vertex data, compared to larger  $x$  data from ZEUS (BPT 97) and NMC. The curves are phenomenological parametrisation of the cross section calculating  $F_2(x, Q^2)$  within the fractal proton structure concept and with different assumptions on  $F_L$ .

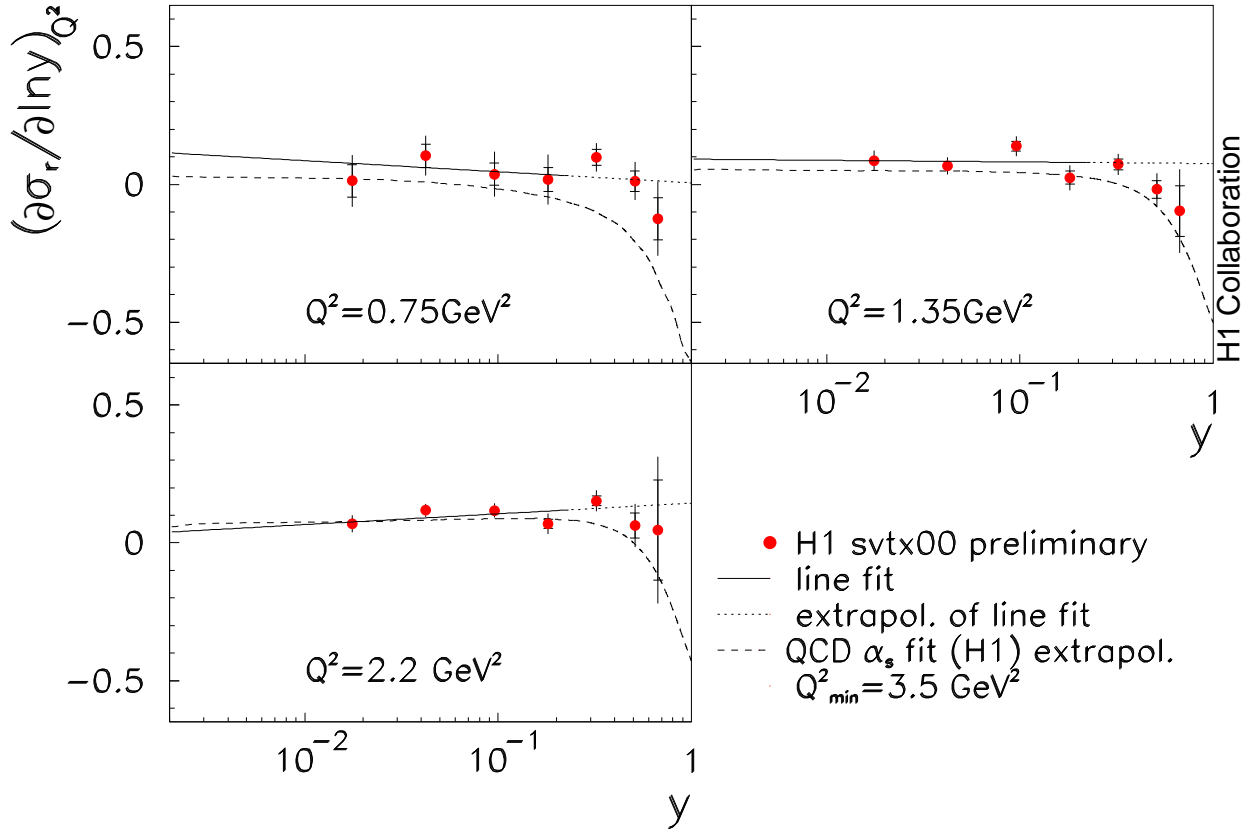


Figure 2: Derivative of the reduced cross section  $\sigma_r$  at fixed  $Q^2$  for shifted vertex 2000 data. The inner error bars represent the statistical errors. The full errors include the statistical, uncorrelated and correlated systematic errors added in quadrature. A linear fit to the low  $y$  points and its extrapolation to the high  $y$  region is shown. In the derivative method, the longitudinal structure function  $F_L(x, Q^2)$  is extracted from the deviation from the linear behaviour in the high  $y$  region according to  $(\partial\sigma_r/\partial \ln y)_{Q^2} = (\partial F_2/\partial \ln y)_{Q^2} - F_L \cdot y^2 \cdot (2 - y)/Y_+^2$ , under the assumption that the linear behaviour of  $\partial F_2/\partial \ln y$  persists in the high  $y$  region. The dashed line represents the QCD fit to previous H1 cross section data extrapolated backwards to  $Q^2$  below  $Q_{min}^2=3.5 \text{ GeV}^2$ .

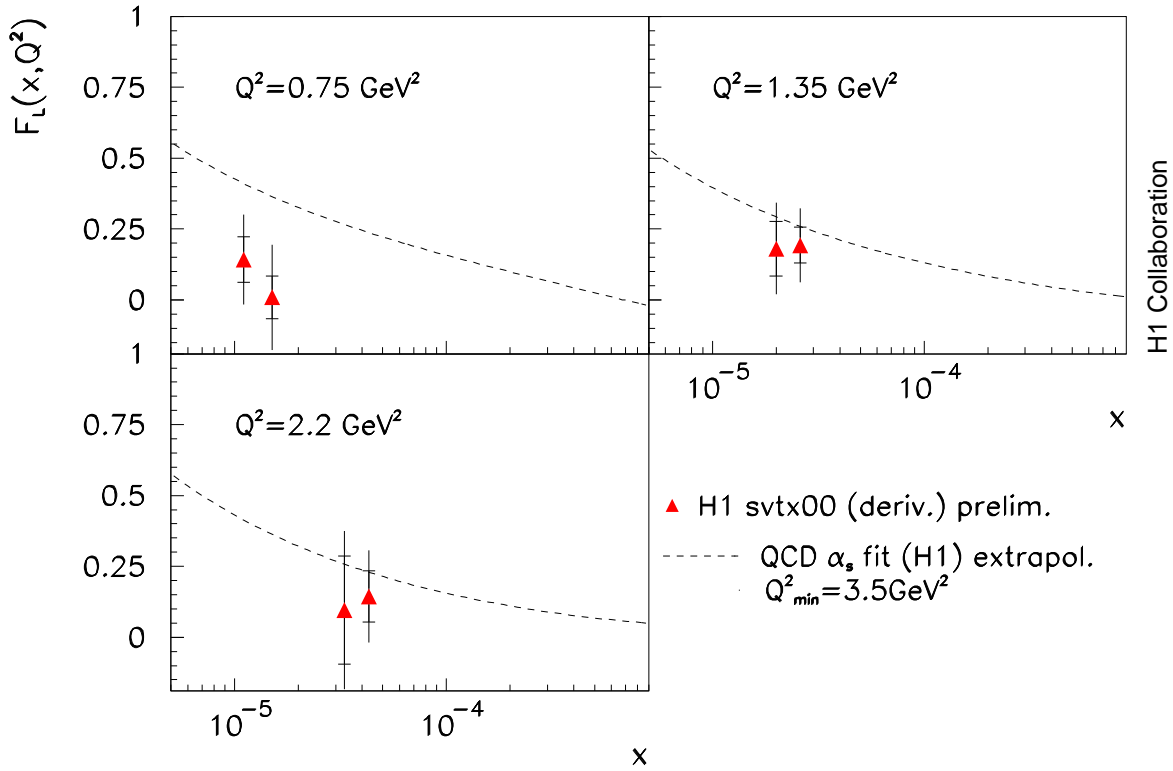


Figure 3: The longitudinal structure function  $F_L(x, Q^2)$  (at fixed  $Q^2$ ) from 2000 shifted vertex data as extracted with the derivative method. The inner error bars represent the statistical errors. The full errors include the statistical, uncorrelated and correlated systematic errors added in quadrature. The dashed line represents the QCD fit to previous H1 cross section data extrapolated backwards to  $Q^2$  below  $Q^2_{\min} = 3.5 \text{ GeV}^2$ .

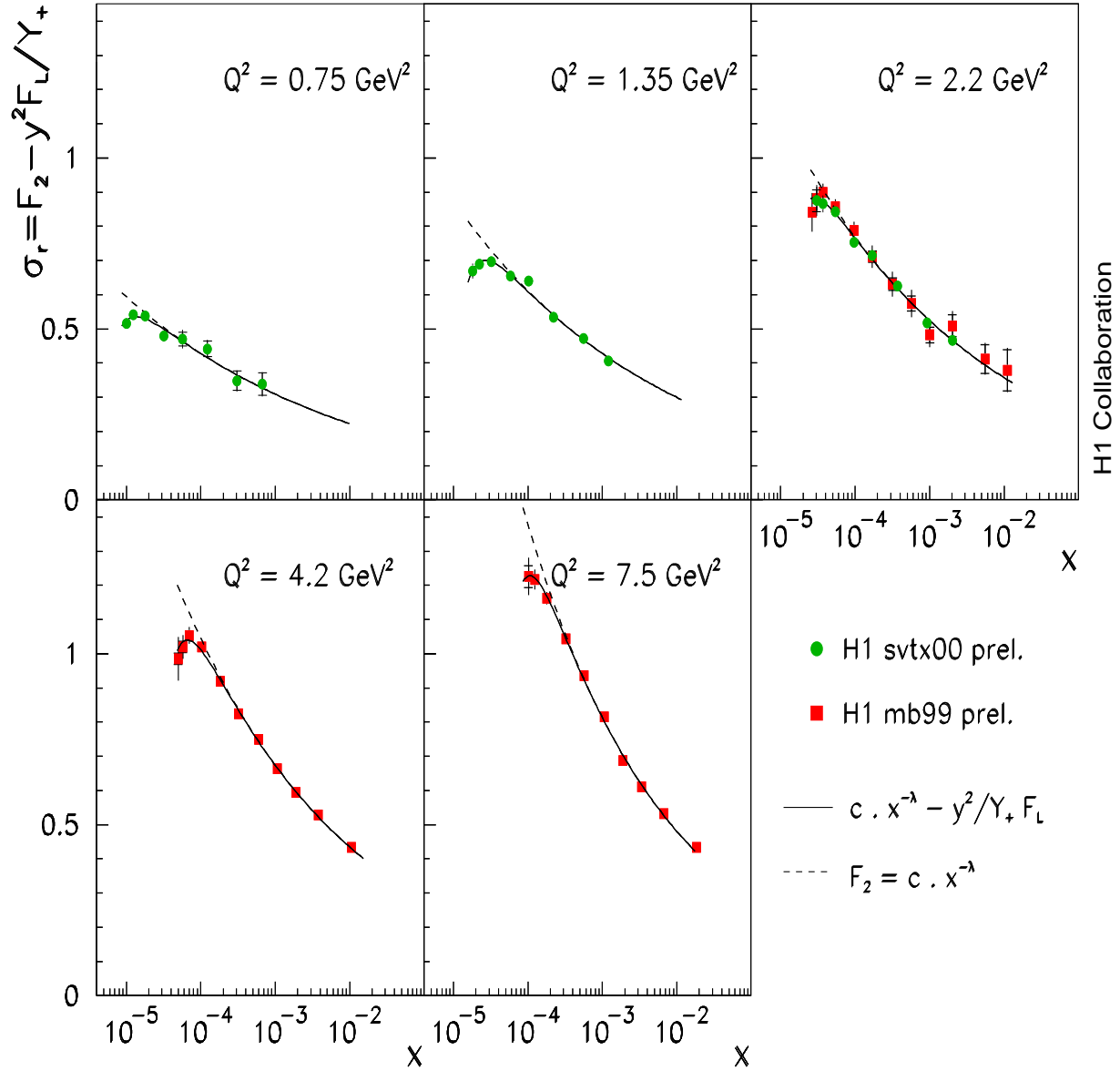


Figure 4: The reduced cross section as a function of  $x$  for different  $Q^2$  bins. Data from 1999 minimum bias (squares) and 2000 shifted vertex (bullets) running periods are shown. The inner error bars represent the statistical errors. The full errors include the statistical and systematic errors added in quadrature. The dashed lines show a function of the form  $\sigma_r = c \cdot x^{-\lambda}$  representing the  $F_2$  contribution to the fitted cross section. The solid lines show fits of the form  $\sigma_r = c \cdot x^{-\lambda} - y^2 / Y_+ F_L$ , from which  $F_L$  is extracted in the shape method.

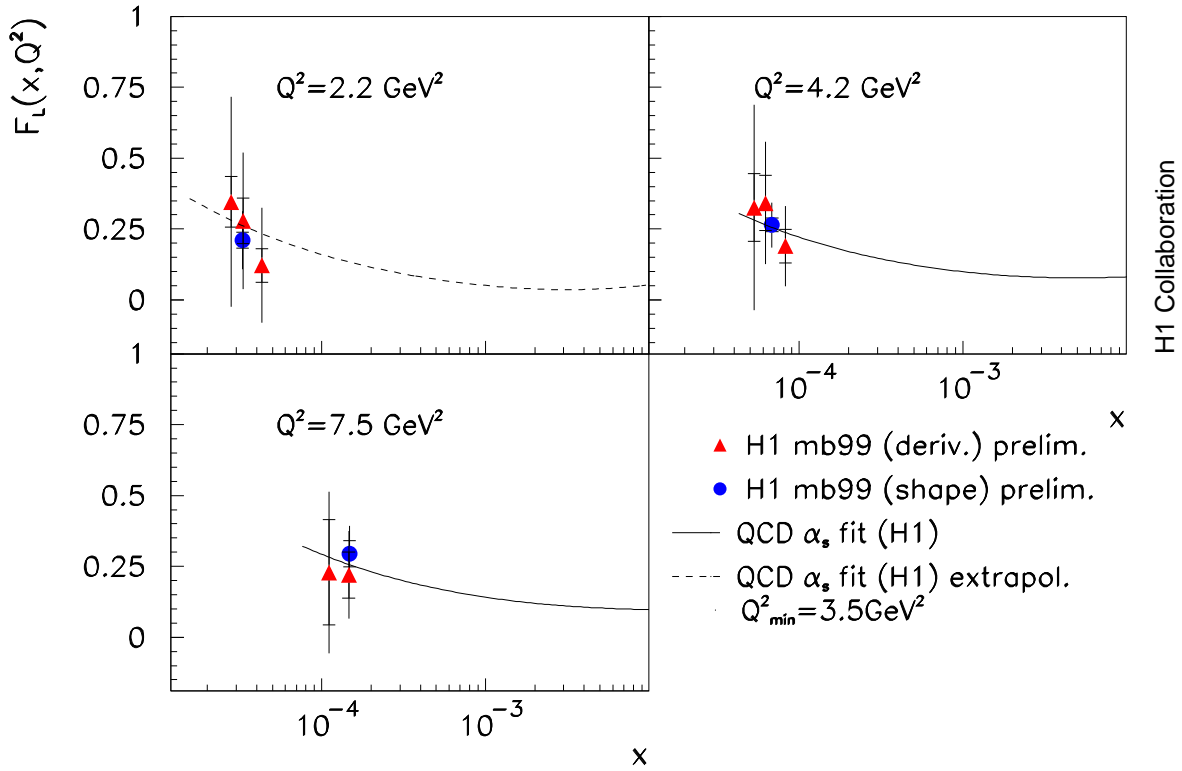


Figure 5: Comparison of  $F_L(x, Q^2)$  results (for fixed  $Q^2$ ) from 1999 minimum bias data as extracted by the derivative (triangles) and shape (bullets) methods. The inner error bars correspond to statistical errors. The full errors include the statistical, uncorrelated and correlated systematic errors added in quadrature. The solid line represents the QCD fit to previous H1 cross section data and the dashed line the QCD fit extrapolated backwards to  $Q^2$  below  $Q_{min}^2 = 3.5 \text{ GeV}^2$ .

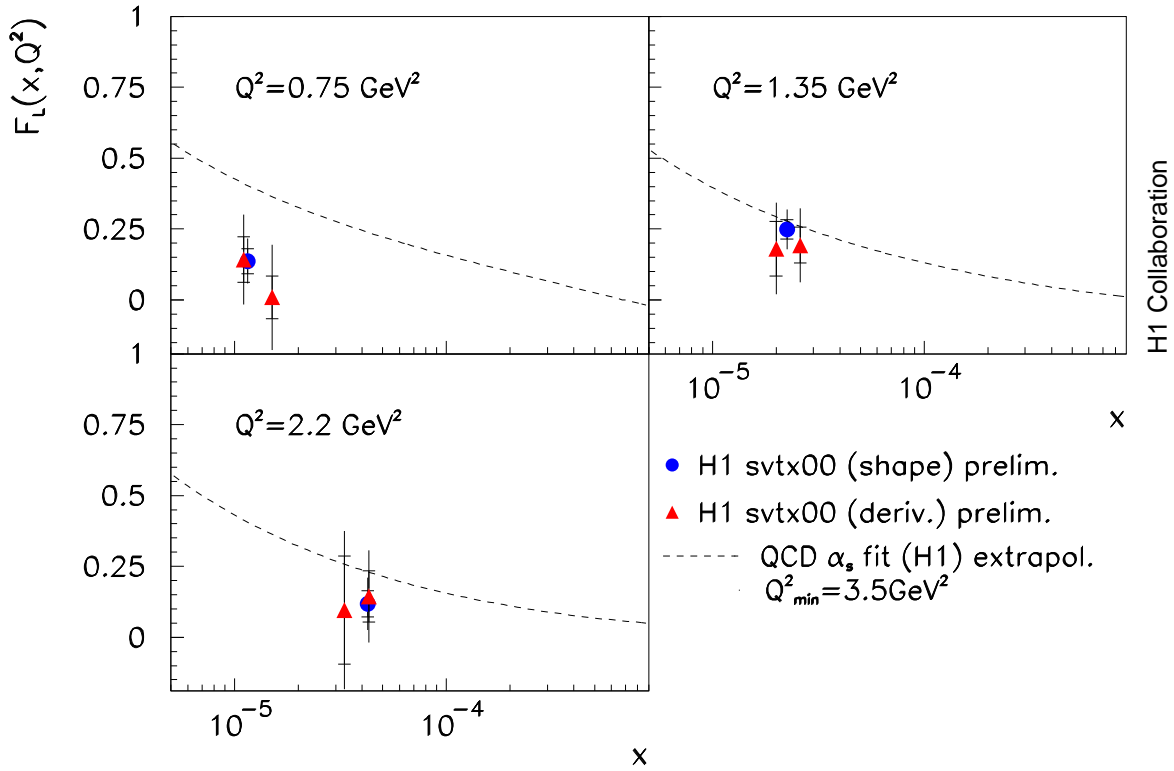


Figure 6: Comparison of  $F_L(x, Q^2)$  results, for fixed  $Q^2$ , from 2000 shifted vertex data as extracted by the derivative (triangles) and the shape (bullets) methods. The inner error bars represent the statistical errors. The full errors include the statistical, uncorrelated and correlated systematic errors added in quadrature. The dashed line represents the QCD fit to previous H1 cross section data extrapolated backwards to  $Q^2$  below  $Q_{min}^2 = 3.5 \text{ GeV}^2$ .

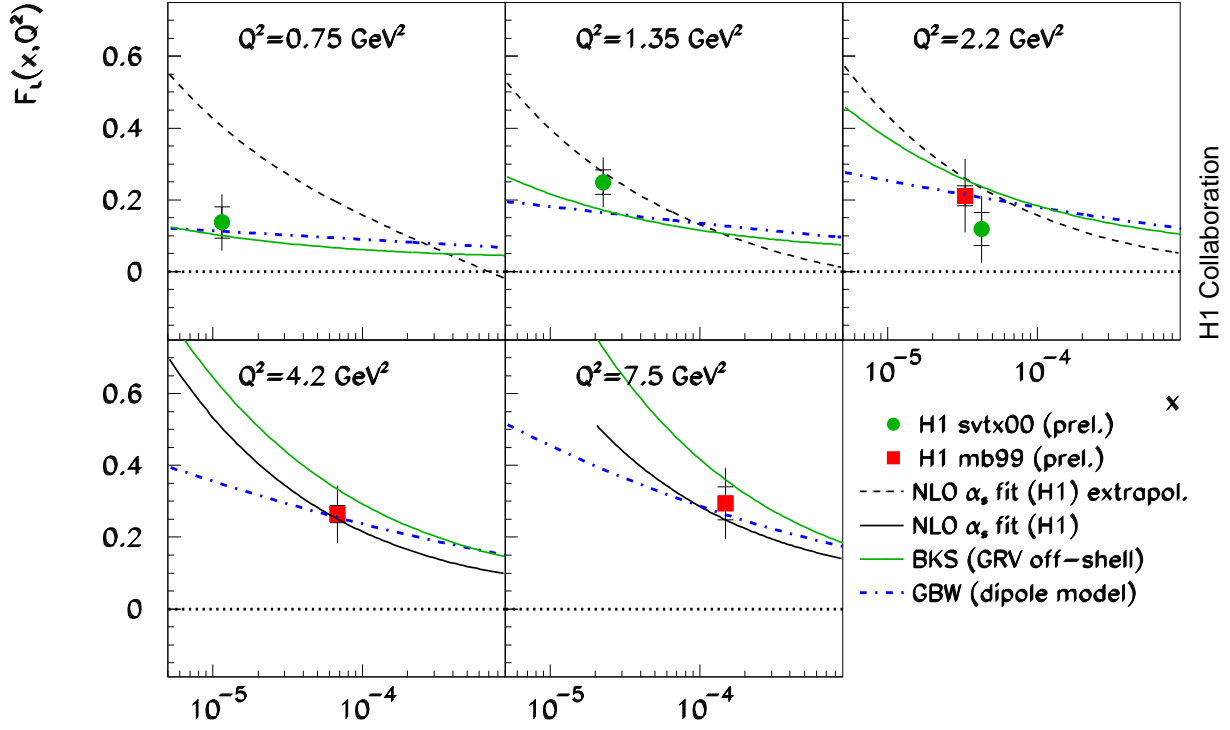


Figure 7:  $F_L(x, Q^2)$ , for fixed  $Q^2$ , from 1999 minimum bias (squares) and 2000 shifted vertex (bullets) data as extracted by the shape method. The inner error bars correspond to statistical errors. The full errors include the statistical, uncorrelated and correlated systematic errors added in quadrature. The solid, black line represents the QCD fit to previous H1 cross section data and the dashed, black line the QCD fit extrapolated backwards to  $Q^2$  below  $Q_{min}^2 = 3.5 \text{ GeV}^2$ . Other curves show predictions of the GBW dipole model [8] (dashed-dotted line) and the BKS model [9] (thin solid, green line).

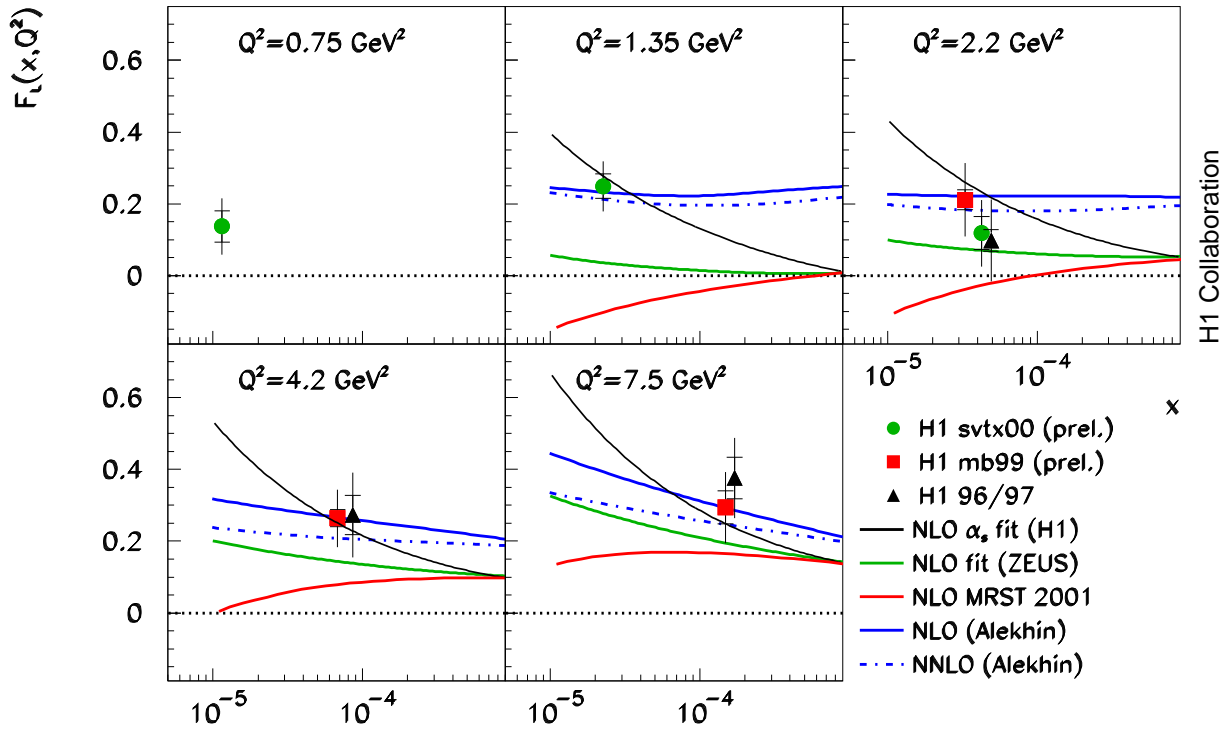


Figure 8:  $F_L(x, Q^2)$ , for fixed  $Q^2$ , from 1999 minimum bias (squares) and 2000 shifted vertex (bullets) data as extracted by the shape method. The inner error bars correspond to statistical errors. The full errors include the statistical, uncorrelated and correlated systematic errors added in quadrature. The solid, black line represents the QCD fit to previous H1 cross section data. The blue lines show results from Alekhin in NLO (solid) and NNLO (dashed). The green line is the result from the ZEUS fit. The red line is the prediction of the MRST 2001 fit in NLO.

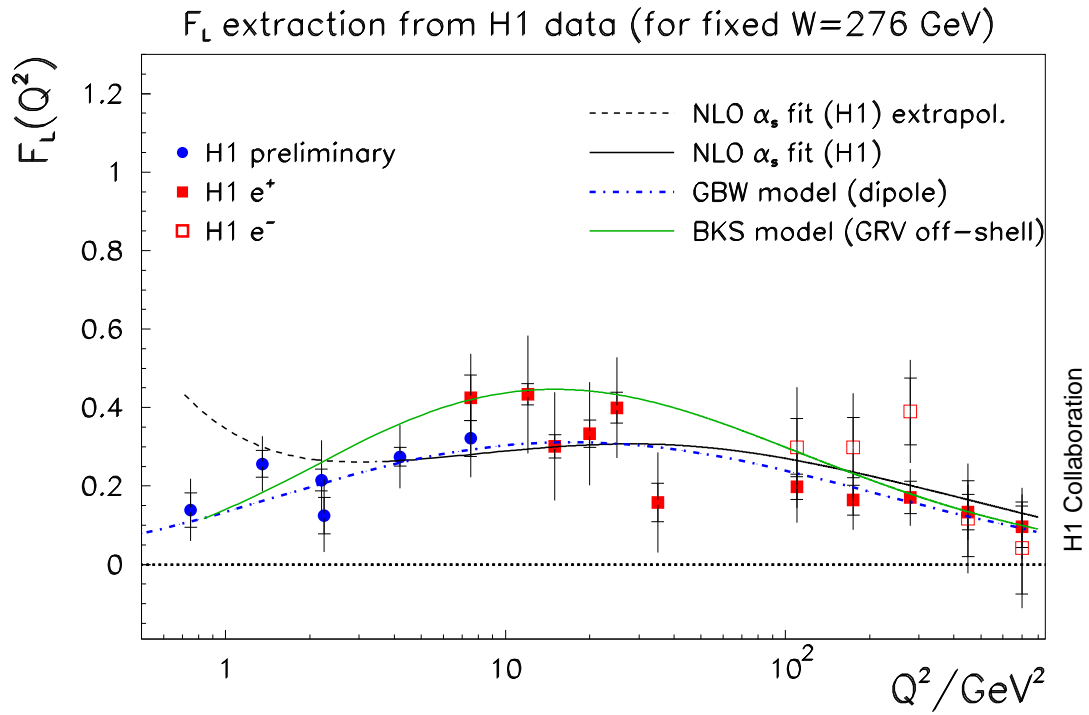


Figure 9:  $Q^2$  dependence of  $F_L(x, Q^2)$  (at fixed  $W=276$  GeV), summarizing the data from the H1 experiment. The inner error bars represent the statistical errors. The full errors include the statistical, uncorrelated and correlated systematic errors added in quadrature. The solid, black line represents the QCD fit to previous H1 cross section data and the dashed, black line the QCD fit extrapolated backwards to  $Q^2$  below  $Q_{min}^2=3.5$  GeV<sup>2</sup>. Other curves show predictions of the GBW dipole model [8] (dashed-dotted line) and the BKS model [9] (thin solid, green line).

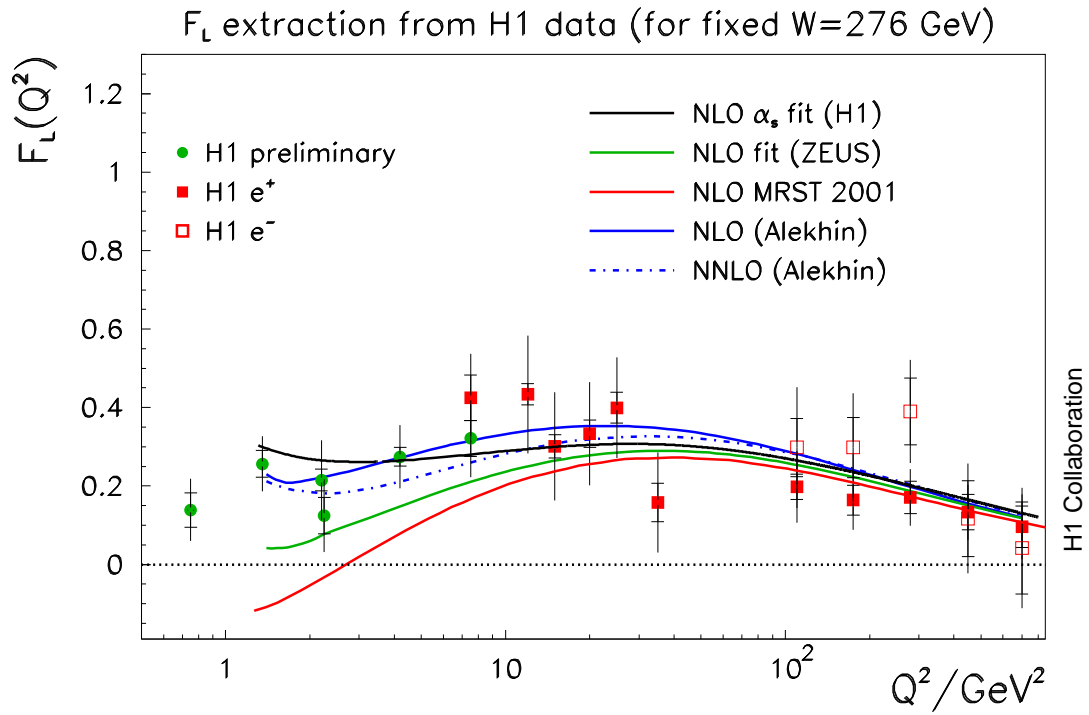


Figure 10:  $Q^2$  dependence of  $F_L(x, Q^2)$  (at fixed  $W=276$  GeV), summarizing the data from the H1 experiment. The inner error bars represent the statistical errors. The full errors include the statistical, uncorrelated and correlated systematic errors added in quadrature. The solid, black line represents the QCD fit to previous H1 cross section data. The blue lines show results from Alekhin in NLO (solid) and NNLO (dashed). The green line is the result from the ZEUS fit. The red line is the prediction of the MRST 2001 fit in NLO.